

DEVELOPMENT OF THE SCANNING FLUID DYNAMIC GAUGE

P.W. Gordon, Y.M.J. Chew and D.I. Wilson

Department of Chemical Engineering and Biotechnology, New Museums Site, Pembroke Street, Cambridge, CB2 3RA, UK
E-mail (P.W. Gordon): pwg23@cam.ac.uk

ABSTRACT

Fluid dynamic gauging (FDG) has been developed to measure both the thickness and strength (cohesive or adhesive) of a range of fouling deposits, *in situ* and in real time, in a liquid environment. We report here the development of the next generation of FDG device, and its application to the study of cleaning on a variety of surfaces. This 'Scanning FDG' allows fully automated movement across a sample surface, enabling spatial distributions of cleaning behaviour to be determined. By allowing measurements to be taken at a variety of points across the deposit, several thickness-time profiles can be recorded in a single experiment. Alternatively, coating patterns can allow different surfaces to be compared under identical conditions. This greatly increases the information that can be obtained from a single experiment, thus reducing the number of experiments required to assemble data sets.

This paper aims to introduce and demonstrate the ability of scanning FDG to study cleaning kinetics of model soils, as well as its potential to measure the adhesive or cohesive strength of a deposit. Its application as a novel imaging technique is used to demonstrate proof-of-concept. Application to commercial cleaning-in-place operations is discussed.

INTRODUCTION

Background

The removal of fouling deposits from process equipment is a chore common to many process industries, from dairy to pharmaceutical manufacture. The ease with which a particular deposit can be removed depends on the cleaning conditions used (*e.g.* temperature, solvent, shear), yet it is also critically dependent on the soil and substrate (*e.g.*, material properties, surface energy, roughness). Improving understanding of cleaning mechanisms (and how the extent of fouling affects cleaning) will enable more targeted fouling mitigation and cleaning procedures. Several attempts have focused on the development of surface treatments and less fouling-prone surfaces, to inhibit attachment of depositing species or by increasing the ease with which they can be removed (Müller-Steinhagen and Zhao, 1997). For instance, surface coatings such as diamond-like carbon have been developed to reduce both the rate of formation of a deposit layer and the force required to remove it (Santos *et al.*, 2004). Additionally, new detergent formulations offer the potential to reduce the

volumes of waste produced and energy consumed during industrial cleaning processes, by operating at lower temperatures or reducing the time required to swell the deposit.

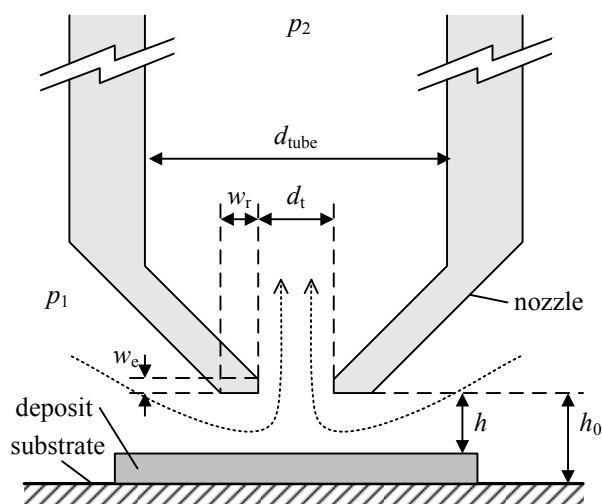


Fig. 1 Schematic of an FDG nozzle. For the scanning FDG, $d_{\text{tube}} = 4$ mm, $d_t = 0.97$ mm, $w_r = 0.465$ mm, $w_e = 0.3$ mm.

In order to compare the efficacy of any of these coatings and formulations, it is necessary to identify parameters which characterise the fouling layer. The most basic parameter of interest is the actual thickness of the deposit film. Since fouling behaviour will change if the deposit is removed from its environment, we want a method which records the thickness *in situ* and in real time. Often the properties of the deposit will change during a fouling/cleaning cycle, so the method should ideally not rely on any particular physical property of the deposit (*e.g.* thermal conductivity) or solution (*e.g.* opacity). A further key property of the deposit is its strength – either adhesive (to the substrate) or cohesive (to itself). These parameters prove difficult to measure using conventional methods, which are often expensive or rely on specific deposit/solution properties.

Fluid Dynamic Gauging (FDG)

Fluid dynamic gauging (FDG) has been developed at Cambridge to allow the study of the swelling and strength of fouling deposits during the cleaning process, *in situ* and in

real time (Tuladhar *et al.*, 2000). This means that the deposit layer is being measured in its natural environment, making extrapolation to real problems much more applicable. A further key advantage over other techniques is the ability of FDG to determine the thickness of a fouling layer locally as a point measurement. The technique makes little fundamental assumptions about the nature of the deposit – in principle any reasonably flat, instantaneously rigid deposit can be investigated. It is a relatively simple and cheap method of gauging and does not require sophisticated sensors. It can be used over a wide range of operating conditions, limited only by the need for a Newtonian, or simple non-Newtonian liquid environment.

Figure 1 illustrates the main principles of FDG. For a fixed pressure driving force ($p_1 - p_2$), the rate of flow into the nozzle, m_{flow} , depends on the nozzle-sample separation, h . By accurate knowledge of the position of the nozzle, h_0 , and measurement of m_{flow} , we can determine the sample thickness, δ , via

$$\delta = h_0 - h \quad (1)$$

where the relationship between m_{flow} and h is determined by calibrating using a clean surface.

Under normal operation FDG can track the thickness and hence swelling of a deposit under cleaning-in-place (CIP) conditions. In an extension to the basic technique, the nozzle can be moved close enough to the sample to impose significant forces upon it (both shear and suction). Once a characteristic yield force is reached, the sample breaks down, providing a measure of the strength of the deposit (Chew *et al.*, 2004b; Hooper *et al.*, 2006). The stresses being imposed by the gauging flow, and hence this characteristic deposit yield force, can be estimated either analytically (Eq. 10) or using computational fluid dynamics (CFD). Details of these simulations can be found in Chew *et al.* (2004a).

This paper will detail the development of the latest FDG apparatus, the scanning FDG (sFDG). In addition to introducing the design and testing of the gauge, several examples of the sFDG operation are reported. These include generating 2D scanning images of a surface profile and tracking the swelling of gelatine and poly(vinyl alcohol) (PVA) deposit layers during soaking in reverse osmosis (RO) water.

EXPERIMENTAL METHODS

Design of sFDG

Figure 2 shows the basic design of the sFDG. The sample is prepared ex-situ, before mounting in place in the sFDG, and exposing to the desired cleaning fluid. As with previous FDG apparatuses, the sFDG uses a siphon action to drive steady flow through the gauging nozzle. The hydrostatic head driving this siphon (H) is set by using a weir to maintain a constant water level in the tank. Temperature control is provided by pre-heating or cooling the inlet feed; operating temperatures from 10 - 50 °C are currently achievable.

The x , y movement is provided by two perpendicular linear slides ($\pm 100 \mu\text{m}$) moving the tank itself rather than

the nozzle. The z -movement is provided via a single linear slide ($\pm 100 \mu\text{m}$) fixed to the nozzle. All x , y and z movement is provided by means of accurate stepper motors (RS 1.8° stepper motor, 12 V). An enclosed balance is used to measure the siphon mass flowrate, m_{flow} . This flowrate is typically calculated based on a 5 - 20 s period, depending on the desired resolution.

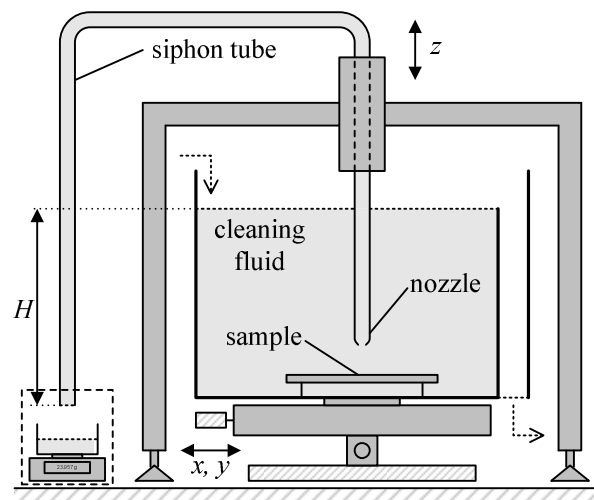


Fig. 2 Schematic of the sFDG. This version of FDG offers the ability to scan across a sample, while still taking measurements *in situ* and in real time.

By being able to monitor the deposit thickness at several different points across the sample in a single experiment, sFDG can generate much more data than previous designs. This enables differences in swelling behavior across a sample to be identified, and conversely it is also possible to use a mosaic of different surfaces to study deposit-substrate interactions, again in a single experiment.

A computer is used to control x , y and z movement, as well as to record the mass flowrate from the balance. For the first time, this enables the actual operation of the gauge to be based on the current behavior of the sample. Specifically, the device uses a feedback system to alter the position of the nozzle (h_0) depending on this siphon mass flowrate. As such, it is possible to keep the nozzle-surface separation, h , constant throughout an experiment, even if the sample is swelling rapidly. This in turn enables the forces (shear or normal) applied on the sample by the gauging flow to be maintained at constant, pre-determined values, or within a set range.

The current design includes a sensitive inductive displacement sensor to give a second, independent measure of z . This gives increased confidence in the value of h_0 , the nozzle-substrate separation. Accurate knowledge of this parameter is crucial if a deposit thickness is to be predicted accurately (Eq. 1).

Calibration and Preliminary Testing

A series of calibration experiments were performed to test the operability and sensitivity of sFDG. For calibration, the nozzle is moved slowly towards a fixed base plate, and the relationship between the mass flowrate, m_{flow} , and the nozzle-surface separation, h , recorded. Typical calibration

curves for two pressure driving forces (H) are shown in Fig. 3.

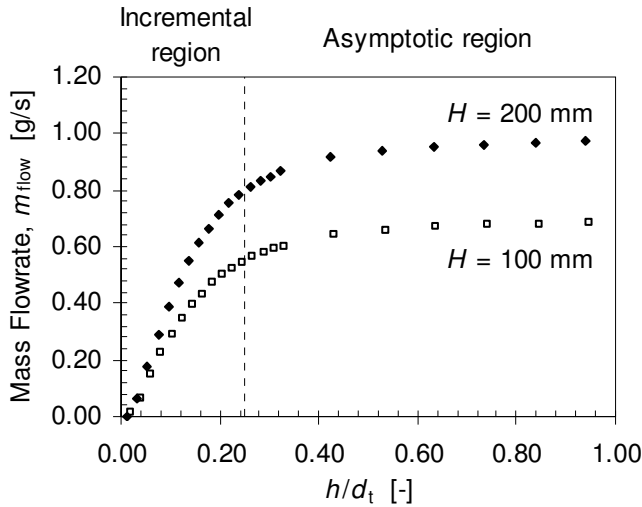


Fig. 3 Typical sFDG calibration curve (RO water, 18 °C). For both thickness and strength measurements, the gauge is used in the incremental region, where m_{flow} is most sensitive to h .

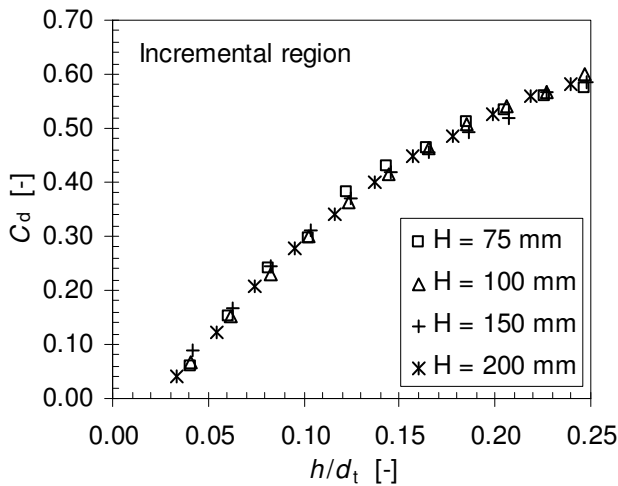


Fig. 4 Effect of h on the discharge coefficient, C_d , for different values of H . Only the incremental region of the calibration curve is shown.

The values of m_{flow} obtained depend on both the pressure driving force in the siphon (H) and the fluid temperature (T). By converting the mass flowrate to a dimensionless discharge coefficient for the nozzle, C_d (Eq. 2), the calibrations for a particular fluid can be collapsed onto a single curve, as shown in Fig. 4. C_d is defined thus:

$$C_d = \frac{m_{\text{flow, real}}}{m_{\text{flow, ideal}}} \quad (2)$$

where, from Bernoulli's equation,

$$m_{\text{flow, ideal}} = \frac{1}{4} \pi d_t^2 \sqrt{2\rho \Delta p_{\text{nozzle}}} \quad (3)$$

Here, d_t is the nozzle inner diameter, ρ is the fluid density, and Δp_{nozzle} is the pressure drop over the nozzle. C_d accounts for all the energy losses associated with flow into and

recirculation in the nozzle. The results in Fig. 4 are similar to those obtained by Tuladhar *et al.* (2000) and Chew *et al.* (2004b), indicating that the sFDG unit is operating properly.

To determine the resolution of the measurements, the gauge was positioned over a clean substrate (no deposit), and the apparent deposit thickness was measured. Fig. 5 shows that the gauge predicts the position of the clean surface to an accuracy of $\pm 5 \mu\text{m}$.

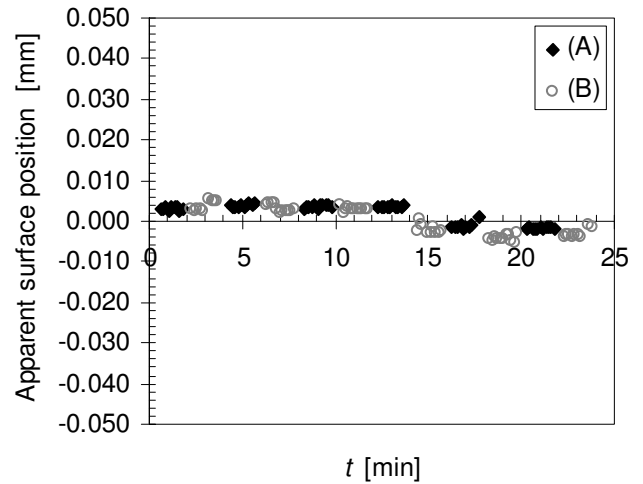


Fig. 5 Resolution test: the gauge locates the position of a static substrate to an accuracy of $\pm 5 \mu\text{m}$. A and B denote two independent points on the surface. The gauge was withdrawn fully between measurements, and the feedback system used to re-locate the surface position: $76 \mu\text{m} < h < 105 \mu\text{m}$ for all measurements.

Surface imaging

The sFDG can also be used as an imaging technique, to view surface profiles for structured deposits or solid substrates. In this way it mimics the operation of an atomic force microscope (AFM), but exploiting fluid mechanical principles and operating on a micron scale. For the initial proof-of-concept investigation, two customized plates were used. The first is a machined brass plate consisting of regular, flat ridges and troughs (Fig. 6). This was used to demonstrate the 1D imaging potential. 2D imaging employed the plate shown on Fig. 7, consisting of vinyl letters glued to a 316 s.s. plate.

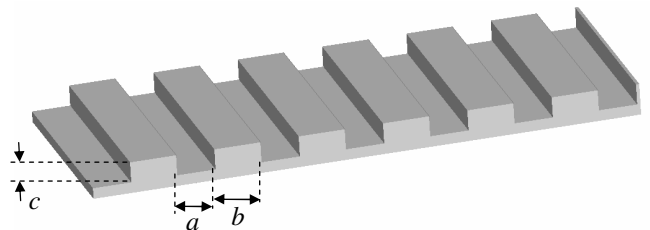


Fig. 6 Crenellated plate used to assess the x resolution of the sFDG. Dimensions $a = 0.84 \text{ mm}$; $b = 0.70 \text{ mm}$; $c = 0.38 \text{ mm}$.



Fig. 7 Patterned 50 mm plate, with ~ 100 μm thick letters.

Materials

The samples used in the deposit swelling experiments were gelatine and PVA. Each was tested as an initially dry deposit, after being challenged by RO water at pH 4.9.

Gelatine samples were prepared by soaking 5.95 g of gelatine (Marks & Spencer fine leaf pork gelatine) in 100 ml RO water, heating gently at 50 $^{\circ}\text{C}$ to dissolve it, before adding 1-2 drops red food colouring (fiesta red, ponceau 4R, E124). The sample plates (316 stainless steel, 50 mm diameter disks) were cleaned by washing with RO water and soaking in acetone, before placing in a 52 mm Petri dish. 12 ml of the gelatine solution was poured over the plates, and this was set by cooling to 2 $^{\circ}\text{C}$ for 5 min. The plate and gel is removed from the Petri dish and dried for 36 h (20 $^{\circ}\text{C}$) before storing chilled. This gave even, dry films approximately 80 μm thick.

PVA samples were prepared by dissolving PVA (Sigma Aldrich, 96% hydrolysed, M_w 85,000 - 124,000) in RO water (60 $^{\circ}\text{C}$) with 90 min sonication in an ultrasonic bath to give a 2 wt% solution. This was then concentrated by evaporation to form a ~ 8 wt% solution. The sample plates were again cleaned as described above prior to deposition. The PVA solution was poured onto the plates to form a layer of ~ 1 mm thick held onto the plate by surface tension. After drying (20 $^{\circ}\text{C}$, 48 h) these yielded films approximately 80 μm thick.

Methods

The swelling experiments reported here were carried out in RO water (pH 4.9), with no agitation other than the small gauging and inlet flows. The zero point, used to find the position of the substrate, was determined immediately following the experiment. Table 1 summarizes the deposits and conditions studied.

Table 1 Deposits studied. Gelatine samples were gauged at several locations on the deposit surface.

Deposit Type	T [$^{\circ}\text{C}$]	H [mm]	Dry Thickness [μm]
Gelatine	20	100	140
Gelatine	30	100	80
PVA	20.5	100	80

CFD SIMULATION

The fluid flow in sFDG was simulated using finite element modeling (FEM) in COMSOL Multiphysics[®] (v3.5). Simulation is feasible here because the device is operated in the laminar flow regime. The governing Navier-Stokes and continuity equations for an axisymmetric incompressible flow of a Newtonian fluid are

$$\text{Navier-Stokes: } \rho(\mathbf{v} \cdot \nabla \mathbf{v}) = -\nabla p + \mu \nabla^2 \mathbf{v} + \rho \mathbf{g} \quad (4)$$

$$\text{Continuity: } \nabla \cdot \mathbf{v} = 0 \quad (5)$$

where \mathbf{v} is the velocity vector, p is the pressure and \mathbf{g} is the acceleration due to gravity.

For a specific geometry (h/d_i), temperature (T) and siphon pressure head (H), simulation yields a value for the mass flowrate through the siphon, m_{flow} . It is convenient to neglect the effect of gravity in the simulation, and instead include its effect in calculation of the pressure driving force.

The pressure driving force from the siphon is hydrostatic, given by Eq. 6. This total pressure drop can be divided into two components; the pressure drop over the nozzle itself (caused by flow contraction and recirculation), and the pressure drop associated with flow along the siphon tube. This latter is described by the Hagen-Poiseuille result (Eq. 7).

$$\text{Siphon hydrostatic head: } \Delta p_{\text{tot}} = \rho g H \quad (6)$$

$$\text{Tube flow: } \Delta p_{\text{H-P}} = \frac{32\mu U L_{\text{eff}}}{d_{\text{tube}}^2} \quad (7)$$

where Δp_{tot} is the pressure driving force in the experiment, $\Delta p_{\text{H-P}}$ is the pressure drop associated with laminar flow in a cylindrical tube, μ is the fluid viscosity, U is the mean velocity in the tube, L_{eff} is the tube effective length, and d_{tube} is the internal diameter of the tube.

The effective length of the sFDG siphon tube, L_{eff} , is 2.10 m. The flow becomes well-established within the first 1 m of the siphon tube, so to simplify the analysis, only 1 m (L_{sim}) of the straight siphon tube was simulated. The pressure drop over the remainder of the tube is given by Eq. 7. This reduces the pressure driving force in the simulation, Δp_{sim} , according to Eq. 8.

$$\Delta p_{\text{sim}} = \Delta p_{\text{tot}} - \frac{32\mu U (L_{\text{eff}} - L_{\text{sim}})}{d_{\text{tube}}^2} \quad (8)$$

The FEM mesh (Fig. 8) was constructed using the in-built software in COMSOL Multiphysics[®], with detailed refinement at the nozzle tip and region immediately downstream of the nozzle where fluid recirculation can occur. Cells in the refined region were 100 times smaller than those in the bulk.

The boundaries are also indicated on Fig. 8, with the specifications given in Table 2. Parameters used in the simulations are detailed in Table 3.

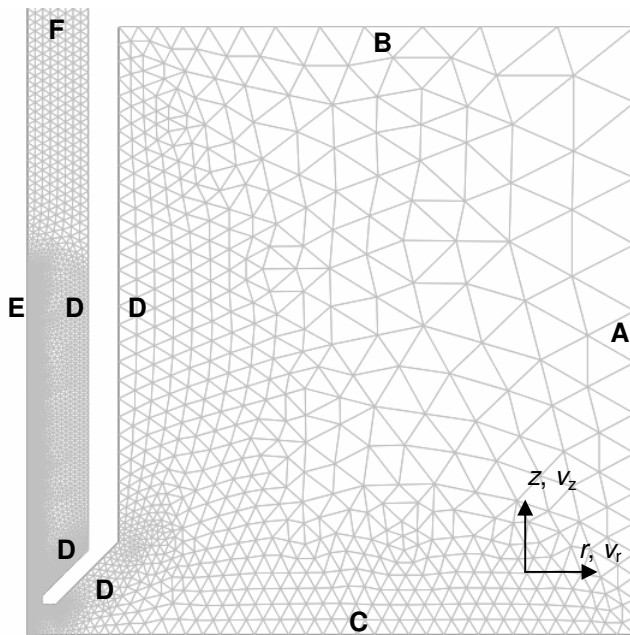


Fig. 8 FEM mesh used in simulations, for $h = 1$ mm. Note that only a small section of the 1 m of siphon tube simulated is shown. Letters denote the boundary conditions.

Table 2 Boundary conditions in CFD simulation.

Domain	Condition
A	Inlet $p = 0$ Streamlines are parallel and normal to the inlet surface, <i>i.e.</i> , $v_z = 0$
B	Pseudo-surface. Beyond this, the flow is assumed not to contribute to the flow through the gauge. At the boundary, the flow is purely axial. <i>i.e.</i> , $v_z = 0$
C, D	Wall. Non-slip and impermeability conditions. <i>i.e.</i> , $v_r = 0, v_z = 0$
E	Axial symmetry. No radial flow across the cell axis, <i>i.e.</i> , $v_r = 0$
F	Outlet. Laminar flow, with velocity profile $v_r = 0, v_z = V_{\max} \left(1 - \frac{r^2}{d_{\text{tube}}^2 / 4} \right)$ V_{\max} , the siphon tube centreline velocity, is given by rearrangement of Eq. 8, where $U = V_{\max} / 2$ for fully-developed laminar flow. $V_{\max} = (p + \rho g H) \left(\frac{d_{\text{tube}}^2}{16\mu(L_{\text{eff}} - L_{\text{sim}})} \right)$

Table 3 CFD simulation parameters.

Parameter	Value
d_t , nozzle internal diameter	0.97 mm
w_r , nozzle rim width	0.465 mm
w_e , nozzle internal edge width	0.30 mm
d_{tube} , tube internal diameter	4.0 mm
L_{eff} , tube effective length	2.10 m
L_{sim} , tube simulated length	1.00 m
ρ , density of fluid, $T = 5$ °C	1000 kg/m ³
ρ , density of fluid, $T = 20$ °C	996 kg/m ³
ρ , density of fluid, $T = 65$ °C	984 kg/m ³
μ , viscosity of fluid, $T = 5$ °C	0.00153 Pas
μ , viscosity of fluid, $T = 20$ °C	0.00103 Pas
μ , viscosity of fluid, $T = 65$ °C	0.00043 Pas

The range of parameters tested was:

$$75 \text{ mm} < H < 200 \text{ mm}$$

$$20 \text{ °C} < T < 65 \text{ °C}$$

$$0.03 < h/d_t < 1$$

Steady-state solution used a parametric linear direct method (PARDISO), taking approximately 30 min to solve (relative velocity vector error $< 10^{-6}$ m/s, which is much smaller than the minimum mean tube velocity of 10^{-3} m/s). Convergence testing was performed by progressively refining the mesh until the solution became independent of cell size. Velocity plots were generated but are not presented. These were identical in form to those reported by Chew *et al.* (2004a).

RESULTS AND DISCUSSION

Experimental and CFD calibration profiles

Figure 9 shows a plot of C_d versus h/d_t from experiments and simulation. The symbol size reflects experimental uncertainty. The results indicate that C_d is independent of both H and T within the range studied. There is good agreement between the simulation and experiment, although the initial gradients differ slightly. This may be due to the edges of the nozzle being slightly rounded or other geometric effects.

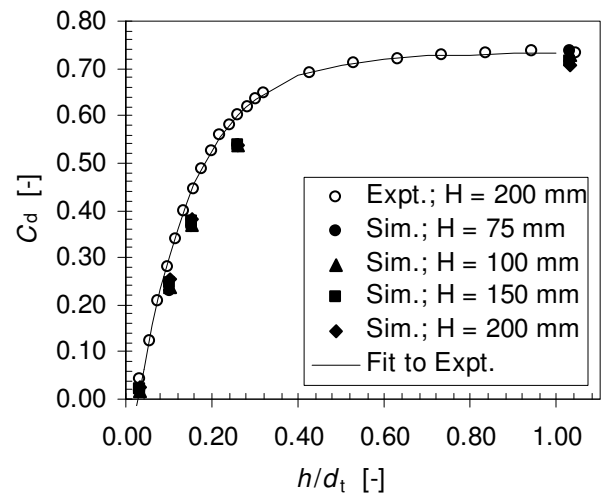


Fig. 9 Comparison of simulation and experiment.

The plot of C_d against h/d_t is now the most general form of the calibration curve. It can be used to predict the relationship between m_{flow} , and h for a given pressure driving force, for a Newtonian fluid, across this temperature (viscosity) range. The locus on Fig. 9 shows the fit for the following function obtained by regression analysis ($R^2 = 0.892$) of the experimental data;

$$C_d = 0.73(1 - \exp(-7.35(h/d_t - 0.027))) \quad (9)$$

Once the gauge has been calibrated, measurement of the deposit thickness, δ , is achieved by a standard method;

- i. Fix the nozzle position, h_o .
- ii. Record m_{flow} over a 5 – 20 s period.
- iii. Calculate C_d , using Eqs. (2) and (3).
- iv. Determine h using Eq. (9).
- v. Calculate δ from Eq. (1).

Surface imaging

The scanning action offers the ability to move between different points on a surface. In order to probe the x resolution of the sFDG, it was used to traverse over the plate shown in Fig. 6, yielding the profile in Fig. 10.

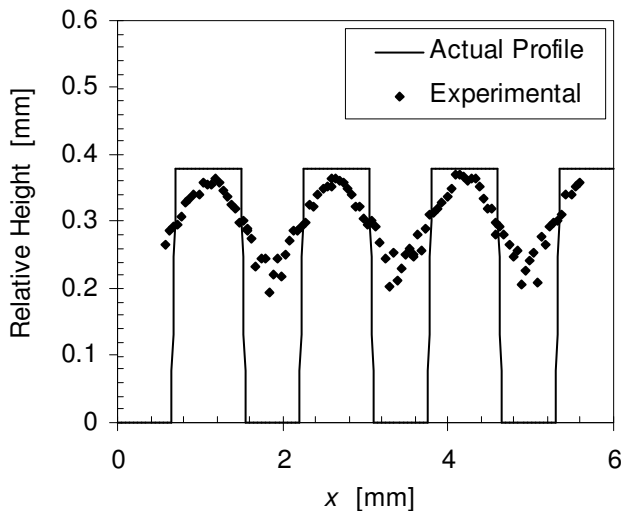


Fig. 10 Relative height of plate in Fig. 6 indicated by the sFDG. Conditions: $H = 200$ mm, $T = 18.8$ °C. Note that the sFDG tip (including rim) is almost 2 mm wide and hence cannot fit into the channels.

Figure 10 indicates that the gauge is able to detect the trenches in the machined plate. Notably, it has difficulty in detecting the step changes in height, and also the true depth of the grooves. This is expected; the nozzle internal diameter is just 1 mm, and so it cannot physically fit inside these grooves. Encouragingly, the scan captures the repeat length of the ridges on the plate.

Another demonstration of the ability of the sFDG to detect a surface profile is the 2D scan of the plate in Fig. 7 presented in Fig. 11. The image was reconstructed based on the values of h . Even this relatively coarse scan (1 mm steps in x and y) was able to form a clear image of the surface, including curvature of the base plate. It should be noted that FDG is not being developed as an imaging tool – this image is merely included here as a proof-of-concept, and a confirmation that the gauge is operating correctly. At

present each scan is relatively time consuming, and there is difficulty in resolving sharp edges.

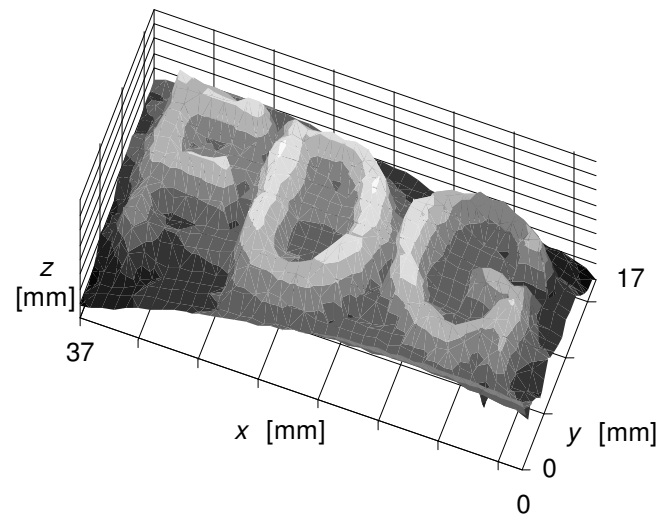


Fig. 11 2-D image of the customized plate in Fig. 7. Contours in z are separated by 0.06 mm.

However, should an application for the imaging be identified, it is believed that both the resolution and the time taken for a scan could be improved relatively easily. The key advantages of such an imaging technique are that it is non-contact, does not rely on the physical properties of the (solid) surface, and can be conducted in completely opaque solutions *in situ*.

Swelling experiments of gelatine and PVA films

FDG has been used previously to monitor the behaviour of a number of food and other soils undergoing chemical cleaning (see Saikhwan *et al.*, 2006). Gelatine and PVA films have been used here as model fouling layers to demonstrate the use of sFDG in tracking the swelling of deposits. In each case, six different points across the sample surface were monitored.

Figure 12(a) shows the swelling of an initially dry gelatine film as it is soaked in water at 20 °C. The film appears by eye to swell uniformly, and this observation is confirmed by the similar rates of swelling exhibited by each of the six points across the sample surface.

In contrast, Fig. 12(b) shows the swelling of a similar gelatine film as it is soaked in water at 30 °C. Initially the rate of swelling is more rapid than at 20 °C. However, at the higher temperature the gelatine was observed to be slowly removed by the small forces applied by the gauging flow. After ~ 5 min the sFDG imposes a sufficient shear force to begin removing the film: the strength of the polymer film depends on the volume fraction of polymer, which decreases as the layer swells. By the time the gauge attempts to measure the thickness of the point (A) for the second time, the sample is too weak, and almost all is removed by the gauging flow before a measurement can be made.

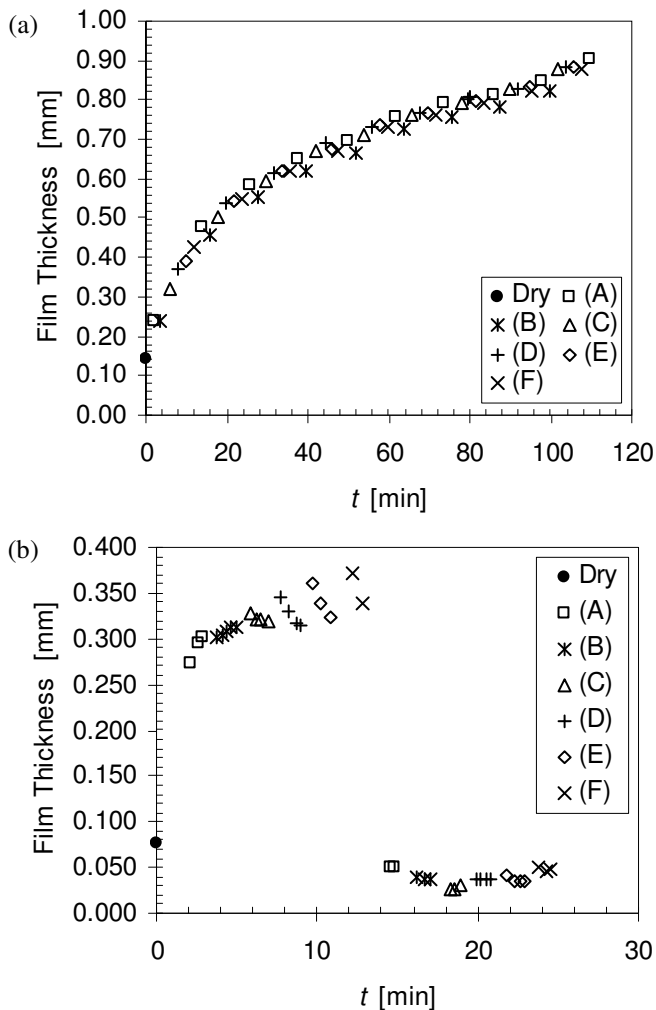


Fig. 12 Swelling of a gelatine film in RO water, pH 4.9. Conditions: (a) 20 °C, dry thickness 140 μm, and (b) 30 °C, dry thickness 80 μm. Thickness was measured using the sFDG at six independent points, denoted A - F, across the sample surface.

The stresses imposed during this experiment can be calculated by simulation or approximated by considering the flow underneath the nozzle rim as a radial flow between parallel disks, *viz.* Middleman (1998)

$$\tau_{\text{wall}} = \mu \left(\frac{3Q}{4\pi(h/2)^2} \right) \frac{1}{r} \quad (10)$$

Here τ_{wall} is the shear stress imposed on the deposit surface, Q is the volumetric flowrate in the tube, h is the nozzle-deposit separation, and r is the radial coordinate.

The above analytical expression is a standard result and its validity for FDG applications is described in Chew *et al.* (2005) and Chew (2004). The shear stress is at a maximum under the inner rim of the nozzle (here, at $r = 0.485$ mm). The shear stress imposed on the layer in Fig. 12(b) was ~ 45 Pa.

The swelling of PVA films has also been monitored using sFDG, as shown in Fig. 13. Initially the deposit swells smoothly, and appears to tend towards an equilibrium thickness. However, after 22 min swelling at 20 °C, the film

was observed by eye to detach from the substrate. This point is characterized by the sudden drop in apparent film thickness. In this case the sFDG is both tracking the swelling and providing a probe into the sample behavior at the surface. The shear stress imposed in this case was ~ 70 Pa.

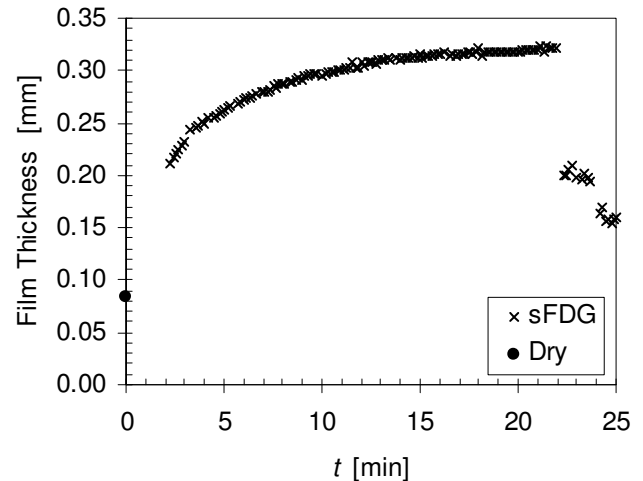


Fig. 13 Swelling of a PVA film, of dry thickness 80 μm, as it is soaked in RO water at 20.5 °C, pH 4.9. The thickness was measured using the sFDG, at a single point on the sample surface.

CONCLUSIONS

- A new scanning fluid dynamic gauge (sFDG) has been constructed, which offers several advantageous features over previous FDG variants.
- The new gauge has been calibrated, and was shown to agree well with CFD model predictions.
- The resolution of the sFDG has been demonstrated to be ± 5 μm. This is better than previous FDG devices, allowing thinner deposit films to be analyzed.
- The potential of sFDG as a novel imaging technique has been demonstrated. The technique is suitable for investigating surface topology on a macroscale. Since the measurement relies only on the gauging flow, it is suitable for use in opaque fluids, does not contact the surface itself, and does not rely on any specific physical properties of the surface.
- The ability of the sFDG to accurately track the swelling of a deposit has been shown using gelatine and PVA films. The sFDG can monitor the swelling of a number of points across the sample during a single experiment, so giving an indication of sample uniformity.
- Further work will now focus on using the sFDG to study the swelling and strength of specific deposits of interest. It will also seek to expand the knowledge of the interaction between gauging flow and the forces applied on the sample via further modeling and experimentation.

NOMENCLATURE**Latin**

a	lined plate trough width, mm
b	lined plate ridge width, mm
c	lined plate ridge height, mm
C_d	nozzle discharge coefficient, dimensionless
d_t	nozzle inner diameter, mm
d_{tube}	siphon tube internal diameter, mm
g	acceleration due to gravity, m/s^2
h	nozzle-sample separation, mm
h_o	nozzle-substrate separation, mm
H	siphon pressure head, m
L_{eff}	siphon tube effective length, m
L_{sim}	simulated siphon length, m
m_{flow}	siphon mass flowrate, g/s
M_w	molecular weight, kg/kmol
p	pressure, Pa
$\Delta p_{\text{H-P}}$	pressure drop due to laminar flow, Pa
Δp_{nozzle}	pressure drop over the gauge nozzle, Pa
Δp_{sim}	simulation pressure driving force, Pa
Δp_{tot}	experiment pressure driving force, Pa
Q	gauging volumetric flowrate, m^3/s
r	radial coordinate, mm
R	sample correlation coefficient, dimensionless
t	time, s
T	temperature, $^{\circ}\text{C}$
U	mean tube velocity, m/s
v	velocity component, m/s
\mathbf{v}	velocity vector, m/s
V_{max}	siphon tube centerline velocity, m/s
w_e	nozzle internal edge width, mm
w_r	nozzle rim width, mm
x	Cartesian coordinate, mm
y	Cartesian coordinate, mm
z	axial coordinate, mm

Greek

δ	deposit thickness, mm
ρ	density, kg/m^3
τ_{wall}	wall shear stress, Pa
μ	viscosity, Pa s

Subscripts

ideal	assuming no losses
r	radial direction
real	experimental
z	axial direction
1	outside the nozzle
2	at siphon tube outlet

ACKNOWLEDGEMENTS

We wish to acknowledge the expertise of Andy Hubbard and Surinder Sall in the construction of the sFDG. In addition, we would like to thank our collaborators at TU Braunschweig (funded by the British Council/DAAD) for assistance with the sFDG testing. EPSRC CASE funding for PWG and Royal Academy of Engineering/ESPRC funding for YMJC is also gratefully acknowledged.

REFERENCES

- Y. M. J. Chew, 2004, Development of fluid dynamic gauging for cleaning studies, pp. 174-176, *PhD Dissertation*, Department of Chemical Engineering, University of Cambridge, Cambridge, UK.
- Y. M. J. Chew, S. S. S. Cardoso, W. R. Paterson, D. I. Wilson, 2004a, CFD studies of dynamic gauging, *Chemical Engineering Science*, Vol. 59, pp. 3381-3398.
- Y. M. J. Chew, W. R. Paterson, D. I. Wilson, 2004b, Fluid dynamic gauging for measuring the strength of soft deposits, *Journal of Food Engineering*, Vol. 65, pp. 175-187.
- Y. M. J. Chew, V. Höfling, W. Augustin, W. R. Paterson, D. I. Wilson, 2005, A method for measuring the strength of scale deposits on heat transfer surfaces, *Developments in Chemical Engineering and Mineral Processing*, Vol. 13 (1/2), pp. 21-30.
- R. J. Hooper, W. Liu, P. J. Fryer, W. R. Paterson, D. I. Wilson, Z. Zhang, 2006, Comparative studies of fluid dynamic gauging and a micromanipulation probe for strength measurements, *Food and Bioproducts Processing*, Vol. 84 (C4), pp. 353-358.
- S. Middleman, 1998, *An introduction to fluid dynamics: principles of analysis and design*, pp. 175-180, Wiley, New York, USA.
- H. Müller-Steinhagen, Q. Zhao, 1997, Investigation of low fouling surface alloys made by ion implantation technology, *Chemical Engineering Science*, Vol. 52 (19), pp. 3321-3332.
- P. Saikhwan, T. Gedert, W. Augustin, S. Scholl, W. R. Paterson, D. I. Wilson, 2006, Effect of surface treatment on cleaning of a model food soil, *Surface and Coatings Technology*, Vol. 201, pp. 943-951.
- O. Santos, T. Nylander, R. Rosmaninho, G. Rizzo, S. Yiantsios, A. Müller-Steinhagen H. Melo-L. Andritsos, N. Karabelas, L. Boulange-Petermann, C. Gabet, A. Braem, C. Trägårdh, M. Paulsson, 2004, Modified stainless steel surfaces targeted to reduce fouling-surface characterization, *Journal of Food Engineering*, Vol. 64, pp. 63-79.
- T. R. Tuladhar, W. R. Paterson, N. Macleod, D. I. Wilson, 2000, Development of a novel non-contact thickness measurement technique for soft deposits and its application in fouling studies, *Canadian Journal of Chemical Engineering*, Vol. 78 (5), pp. 935-947.